Design and *In Vivo* Test of a Batteryless and Fully Wireless Implantable Asynchronous Pacing System

Sajid M. Asif*, *Student Member, IEEE*, Jared Hansen, *Student Member, IEEE*, Muhammad S. Khan, *Student Member, IEEE*, Scott D. Walden, Mark O. Jensen, Benjamin D. Braaten, *Senior Member, IEEE*, and Daniel L. Ewert

***Abstract*— *Goal*: The aim of this study is to develop a novel fully wireless and batteryless technology for cardiac pacing. *Methods*: This technology uses radio frequency (RF) energy to power the implanted electrode in the heart. An implantable electrode antenna was designed for 1.2 GHz; then, it was tested *in vitro* and, subsequently, integrated with the rectifier and pacing circuit to make a complete electrode. The prototype implanted electrode was tested *in vivo* in an ovine subject, implanting it on the epicardial surface of the left ventricle. The RF energy, however, was transmitted to the implanted electrode using a horn antenna positioned 25 cm above the thorax of the sheep. *Results*: It was demonstrated that a small implanted electrode can capture and harvest enough safe recommended RF energy to achieve pacing. Electrocardiogram signals were recorded during the experiments, which demonstrated asynchronous pacing achieved at three different rates. *Conclusion*: These results show that the proposed method has a great potential to be used for stimulating the heart and provides pacing, without requiring any leads or batteries. It hence has the advantage of potentially lasting indefinitely and may never require replacement during the life of the patient. *Significance*: The proposed method brings forward transformational possibilities in wireless cardiac pacing, and also in powering up the implantable devices.**

***Index Terms*—Energy harvesting, implantable antennas, impantable electronics, pacemakers, radio frequency.**

I. Introduction

CARDIAC resynchronization therapy (CRT) devices are of significance in the current era, as they have the potential to greatly improve patient outcomes. Today, more than three million people worldwide have a pacemaker and its need is even increasing, as heart failure (HF) alone affects more than 5.1 million people in the United States and 25 million worldwide [1]. Although the conventional cardiac pacemakers improve the quality of life and reduce mortality, there are problems associated with them, due to many potential procedure- and device-related complications [2]. Among all components, the pacing lead is considered to be the weakest link of the cardiac pacing system, but serves as a conduit for the delivery of energy pulses to provide myocardial stimulation [3]. Leads can produce venous obstruction and are prone to insulation breaks, conductor fracture, and even infection [4]–[7]. In addition to the lead complications, CRT is currently delivered epicardially via the coronory sinus, whose anatomy can make implantation difficult to achieve the optimal pacing site [8].

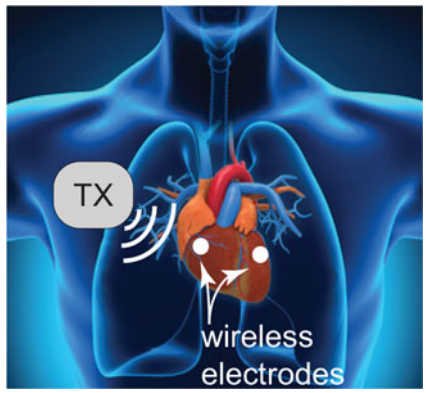

Fig. 1. Conceptual diagram of the proposed wireless cardiac pacing system. The transmitter (TX) placed above the thorax sends RF energy to the implanted electrode in the heart, which converts it into DC power by the on-board rectenna. This power is used by the pacemaker to stimulate the heart tissue (figure adapted from [9]).

Inductive radio frequency (RF)-based pacemakers were first reported in [10] and [11]. Very recently, the first ever implantation of leadless endocardial pacing using ultrasound was performed on humans [12]. Also, St. Jude [13] and Medtronic [14] have recently been developing miniaturized prototype pacemakers, which are currently going through clinical trials in Europe and the USA. Both St. Jude's Nanostim and Medtronic's Micra Transcatheter Pacing System are the latest innovative devices for implantation in the right ventricle. However, there is still a need for a batteryless device, which would potentially make multiple site pacing practical and address the unmet clinical needs of the CRT nonresponders.

The objective of this paper is to propose and demonstrate a novel method of leadless cardiac pacing, as shown in Fig. 1. This does not require leads or electrode batteries and has the ability to pace multiple sites of the heart, not just a single chamber. This

Manuscript received June 4, 2015; revised August 14, 2015; accepted August 31, 2015. Date of publication September 9, 2015; date of current version May 19, 2016. This work was supported in part by the North Dakota Department of Commerce under the ND Venture Grant 14-08-J1-66 and in part by the US National Science Foundation under the ND EPSCOR INSPIRE-ND Grant IIA-1355466. *Asterisk indicates corresponding author.*

*S. M. Asif is with the Department of Electrical and Computer Engineering, North Dakota State University, Fargo, ND 58102 USA, and also with the Department of Electrical Engineering, COMSATS Institute of IT, Attock 43600, Pakistan (e-mail: sajid.asif@ndsu.edu).

J. Hansen, B. D. Braaten, and D. L. Ewert are with the Department of Electrical and Computer Engineering, North Dakota State University

M. S. Khan is with the Department of Information Engineering, University of Padova.

S. D. Walden is with the Department of Animal Nutrition and Physiology Center, North Dakota State University.

M. O. Jensen is with the Department of Surgery, University of North Dakota School of Medicine and Health Sciences.

Color versions of one or more of the figures in this paper are available online at http://ieeexplore.ieee.org.

Digital Object Identifier 10.1109/TBME.2015.2477403

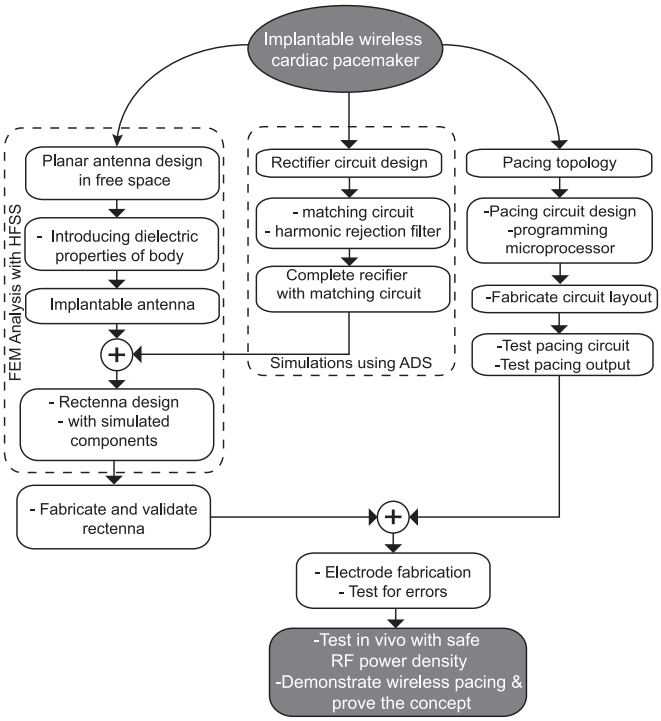

Fig. 2. Flow diagram for the design, analysis, and test of the proposed RF-powered wireless cardiac pacemaker system.

is achieved by exploring the integration of implantable antennas with radio frequency (RF) energy harvesting techniques to power the pacemaker for myocardial stimulation. The proposed solution has a significant advantage over all the aforementioned methods because batteries are not required for the operation of the implanted electrodes, which saves almost half of the available space. Furthermore, the proposed technology has a significant advantage over the ultrasound based system because it is completely wireless and allows multiple electrodes to be implanted without a pulse generator or pacemaker lead. Moreover, this technology allows the flexibility of pacing multiple sites of the heart without the need of any leads.

In particular, this study presents the design and demonstration of a complete wireless and batteryless electrode for cardiac pacing. The electrode is comprised of an implanted rectenna, an impedance matching circuit, and a charging circuit, as well as a microprocessor-based pacing circuit. A detailed flow diagram of the system design is depicted in Fig. 2. A planar microstrip receiver antenna with complimentary split ring resonator-loaded ground plane was first optimized for the miniaturization and then matched with an efficient rectifier circuit for maximum power transfer between the rectenna and the pacing circuit. A ceramic capacitor was used to store the charge before delivering it to the pacing circuit to provide pacing and stimulate the tissue. The two-layer wireless electrode prototype was fabricated in house and enclosed in a small enclosure. Finally, the wireless electrode was tested *in vivo* (ovine subject) to validate the concept and demonstrate the pacing. The electrocardiogram (ECG) results showed that the pacing was achieved at three different rates: 110, 120, and 130 beats/min (bpm).

Implantable antennas and energy harvesting for the implantable biomedical devices exhibit numerous challenges in terms of design, fabrication, and testing, as summarized in [15]–[17]. The guidelines for designing implantable antennas in different environments are presented in [18] and [19]. Many researchers have designed and developed different types of antennas for implantable applications including planar loops, inverted-F, monopoles, dipoles, spirals, meanders, and microstrips antennas [15], [20]–[32]. For many years, inductive telemetry has been used to power pacemakers [33] and for data transmission in implantable applications [34], [35], but its uses have been limited by the quality and size of the implanted coil. For cardiac telemetry, a dipole [21] and microstrip [22] embedded in the shoulder were analyzed using the finite-difference time-domain method. Recently, the use of preexisting vascular stents as antennas have been examined, but no *in vivo* results have been presented [24], [25]. Although the stent-antenna uses preapproved biocompatible materials, it is still not ready for use in certain vessels, and hence, not recommended to be used in the heart chambers [25]. A miniaturized circularly polarized microstrip antenna has recently been tested in pork for implantable applications [36].

The key components of an implantable rectenna are the implantable antenna, rectifier circuit, and matching circuit. An efficient rectenna is crucial for the delivery of wireless power [32], [37]–[46]. While there has been a huge interest in the rectennas for air, limited work has been reported for implantable applications. An implantable rectenna design for triple-band biotelemetry communication has been demonstrated *in vitro* [43]. Marnat *et al.* designed an on-chip antenna for wireless power and data transfer for the implantable intraocular pressure monitoring applications [42]. A flexible dipole rectenna array fabricated on a cellulose membrane has been proposed for the biomedical applications, but has a large size and only 56% conversion efficiency [47]. Recently, a miniature energy harvesting rectenna using Planar inverted-F antenna and a spiral design was proposed for deep brain stimulation, but no *in vivo* results have been shown [48]. Previous studies described in [25] and [49] used ANSYS High Frequency Structure Simulator (HFSS) and conducted *in vivo* experiments to validate the power transfer from a stent-based radiator implanted deep within the body.

This paper is structured as follows: Section II is a preliminary section, in which the system design topology and its constraints are presented. Section III is dedicated to the selection and design of the implantable antenna, its concepts, workings, and parametric analysis. Section IV discusses the topology of the rectifier circuit and its efficiency, as well as illustrates the full schematic of the system. Section V describes the pacing circuit and the load, while Section VI explains the validation and fabrication of the prototype. Measurement and *in vivo* surgeries are described in Section VII, while results and discussions are summarized in Section VIII. The paper ends with a conclusion and future study recommendations in Section IX.

II. System Design Topology and Physical Constraints

The topology configuration of the proposed implantable electrode for cardiac pacing is shown in Fig. 3. Designing a system with an antenna for use in the deep human body is comparatively different and more complex than designing it for air or

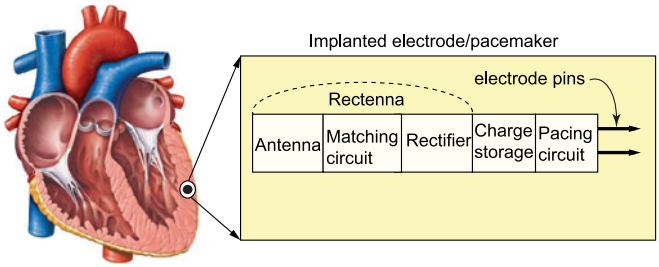

Fig. 3. Proposed location for implanting the wireless electrode and system topology, with all the parts depicted in order [50].

subcutaneous applications, due to the physical constraints and electromagnetic specifications. As shown in Fig. 3, the antenna is not the only implant, but is a part of the complete active implantable system. Hence, it needs to be miniaturized without compromising on its gain. Critical to its practicality, the volume of this system must be small and able to fit in a small housing. Furthermore, since the human body tissue is highly conductive and prone to the adverse tissue reaction, the device has to be embedded well in a biocompatible insulation to avoid these issues [51]–[53]. Compact packaging is also required to reduce the overall volume. The complete system is hence designed in layers as discussed in Section VI. It should be noted that the actual antenna manufacturing process has limitations too, which have to be considered during the simulation and optimization stage.

III. Implantable Antenna Design

This section describes the realization of an efficient implantable antenna at 1.2 GHz.

A. Design Methodology and Selection of the Antenna

The intended goal was to design a linearly polarized antenna at 1.2 GHz for implantation on the heart tissue, deep inside the body. Considering the overall volume of the electrode, the antenna dimensions were set to 10×10 mm^2. To overcome all the physical and design constraints, the following design procedures were followed:

1) The antenna was designed in free space without considering any dielectric substrates and phantoms. This process helped in reducing the simulation time and allowed an approximation to select an efficient design.
2) The excitation methods were investigated and the antenna topology was selected accordingly.
3) The antenna design was tuned after adding the dielectric substrate and body phantom.
4) The antenna structure was modified to integrate the matching and rectifier circuit.

These steps are helpful to understand how the final antenna structure was developed and achieved. Besides the miniaturization and biocompatibility, the selected antenna model should allow extensive parametrization and a good degree of freedom in the design. An extensive study of the antenna designs, such as meander line, spiral, multilayered and microstrip patch, was performed to choose an antenna structure that was efficient for the given volume and that had a fast computational performance

TABLE I
Tissue Electric Properties at 1.2 GHz

Permittivity (ε_r)	Conductivity (σ [S/m])	Loss tangent	Mass Density (ρ [kg/m^3])
53.4	1.0554	0.2904	1040

(in free space). Following the analysis of the radiation characteristics and the concept of current distribution of these antennas [54], a microstrip patch was selected. Microstrip patch design has a good history in implantable applications and provides flexibility in the design, shape, and conformability, as reviewed in [15]. The use of a patch antenna allows several miniaturization techniques [53] that can be employed to achieve the required size and resonance frequency. The antenna having to be implanted into the heart tissue helped further in miniaturization because tissue has a higher dielectric constant than fat.

B. Human Body Model and Numerical Methods

Many possibilities of the equivalent body models are available with different complexities, as reported in [55]–[57]. Realization of a single body phantom for different frequency ranges is complex [58], and hence, a broad frequency range was achieved only with equivalent properties of a skull in [59]. Following the recommendations in [60], a simple homogeneous cylinder with values of dielectric properties of the muscle [61], [62] is used in this study. This is an approximation but it does provide a standard and is useful to realize conditions for the antenna measurements in less time [63]. The electric properties of the tissue model used in the simulations at 1.2 GHz are given in Table I.

Performance of the antenna was examined using the properties given in Table I. The antenna was implanted 6 cm under the skin, deep inside the tissue, with its ground being placed on the heart's surface. All the simulations were performed using a full-wave 3-D electromagnetic simulation tool, Ansoft's-ANSYS HFSS, which enabled efficient modeling of anatomical body parts. To achieve the stability of the numerical calculations and extend the radiation infinitely far, the absorbing boundaries were set at $\lambda_0/2$ away from the antenna in the simulation setups.

C. Miniaturization of the Antenna Using CSRRs

Complimentary Split Ring Resonators (CSRRs) have attracted much attention and have been used extensively due to their metamaterial properties and attractive performance characteristics [64]. Applications of metamaterials in medical imaging, microwave hyperthermia, wireless strain sensing, and specific absorption rate reduction have been reviewed recently in [65]. Applications of CSRRs for miniaturization and improving directivity have been investigated in [66]. The CSRR unit cell was introduced in the ground to miniaturize the antenna, which also facilitated a good impedance match to the source, a nearly broadside radiation pattern, and a high radiation efficiency. In addition to CSRR, several other methods have been presented in the literature to reduce the size of patch antennas, including the use of shorting posts [67], loading of reactive elements [68],

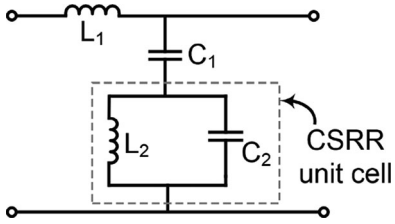

Fig. 4. Equivalent circuit model of the CSRR unit cell [64].

and the use of reactive impedance surfaces [67]. An investigation into the design of compact patch antenna loaded with CSRR and reactive impedance surfaces, together with their performance analysis has been reported in [69]. Very recently, a combination of CSRRs and reactive pin loading has been presented in [70], which demonstrated a size reduction of 30% and 44% while using CSRR alone and with the addition of active pins, respectively.

Unlike the study reported in [66], Cheng *et al.* proposed the use of a CSRR in the radiating patch instead and designed a compact patch antenna for wireless endoscopy [71]. Despite its proposed implantable application, the body dielectric properties were not considered in this design and also no *in vitro* or *in vivo* results were measured. A similar concept of miniaturization using the CSRR is employed in our study. We have also considered the equivalent body model with correct dielectric properties, which strongly influences the antenna design.

D. CSRR Unit Cell

The metamaterial property of the CSRR unit cell (i.e., its negative permittivity and left handed propagation) has been realized in [64]. It is an electrically small resonator that operates as an *LC* tank circuit with a high Q-factor, the equivalent circuit model for which is shown in Fig. 4. Since the electrical length of a metamaterial unit cell is much smaller than the wavelength of the operating wave, the CSRR becomes a useful tool for miniaturization. Changing the physical size of the CSRR unit cell changes the L_2 and C_2, as given by:

$$f_0 = \frac{1}{2\pi\sqrt{L_2 C_2}} \tag{1}$$

The desired resonant frequency, hence, can be achieved by controlling the L_2 and C_2. The layout of a patch antenna loaded with an optimized CSRR unit cell at 1.2 GHz and its dimensions are illustrated in Fig. 5. This design layout was achieved after extensive parametrization, summarized in the next section.

E. Parametric Analysis

In the first attempt, a 50 Ω matched microstrip patch antenna was designed within a 8.5 $\times$ 9.8 mm^2 area, which resonated at 4.6 GHz. As shown in Fig. 6(a), no CSRR loading was employed in this case. Various dimensions of the CSRR were tested at all the practical locations on the ground plane to see its effects and changes on the antenna performance. Several combinations of these geometries together with the resonant frequencies are

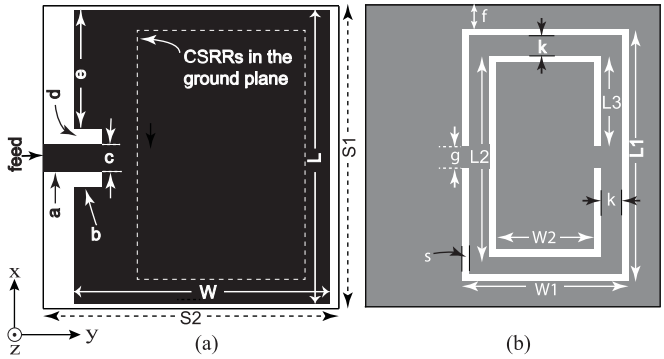

Fig. 5. Geometry of the optimized patch antenna loaded with CSRR in the ground plane. (a) Top view and (b) bottom view. Structure characteristics are (in mm): $a = 2.3$, $b = 1.1$, $c = 1.2$, $d = 0.5$, $e = 3.8$, $W = 8.5$, $L = 9.8$, $S_1 = 10$, $S_2 = 10$, $f = 0.5$, $g = 0.6$, $s = 0.25$, $L_1 = 9$, $L_2 = 8$, $W_1 = 6.57$, $W_2 = 4.5$, $L_3 = 3.7$.

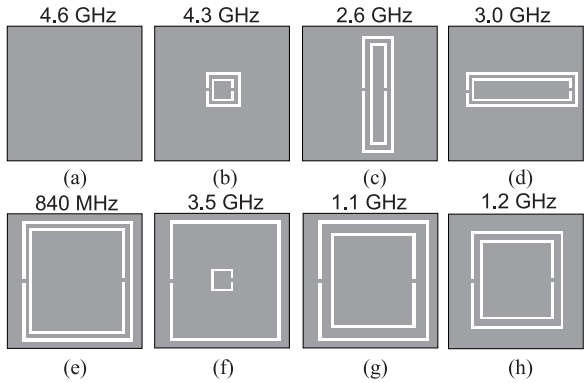

Fig. 6. Different geometries of the CSRRs (etched in the ground plane of the same antenna), resulting in different resonant frequencies.

shown in Fig. 6(b)–(h). It should be noted that the substrate material used in the HFSS simulations was Rogers TMM10i.

Initially, the CSRR was etched exactly below the center of the patch with the smallest possible dimensions ($L_1 = 3.5$ mm, $W_1 = 2.5$ mm), that can be milled in house. No significant frequency shift was observed but it did, however, seem to be an effective method. Putting the CSRR at the center location, as shown in the Fig. 6(b), provided maximum flexibility for the parametrization analysis. In order to better understand the effect of each parameter on the resonant frequency and miniaturization, let us consider the following cases:

1) *Case I—Variations in the widths:* The widths W_1 and W_2 of the CSRR were extended from the center to the maximum value (W), while keeping all the other parameters constant. As a result, the resonance frequency got shifted to the lower band as the width increased but it was not very effective to achieve a resonance below 3 GHz, as shown in Fig. 6(d).
2) *Case II–Variations in the lengths:* Next, the lengths L_1 and L_2 of the CSRR were increased, while keeping all the other parameters constant. This method revealed a better shift in the resonance to the lower band, as frequency as low as 2.6 GHz was achieved in this case, as shown in Fig. 6(c).

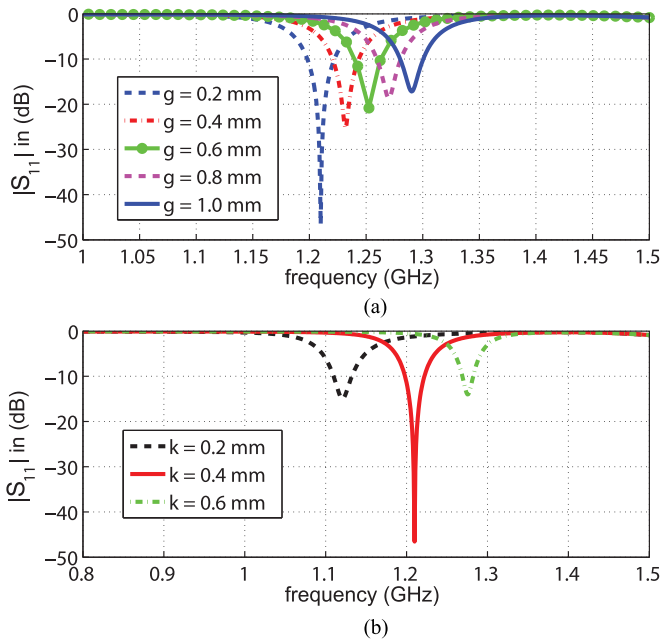

Fig. 7. Results of the parametric analysis of the antenna. (a) Variations of the space (g), and (b) variations of the gap (k) in the CSRR.

3) *Case III—Variations in the lengths and widths together:* Following the first two cases, the lengths and widths of the CSRR were then increased proportionally and found to be an effective method to achieve a lower resonance. The maximum practical dimensions of the CSRR, as shown in Fig. 6(e), helped the antenna resonated at 840 MHz. The parameter, *"g"* however played an important role in achieving a good match at this frequency.
4) *Case IV—Variations in the gap, "g":* This was an important parameter in the CSRR unit cell. Fig. 7(a) shows the results of the implantable antenna with variations of the gap *"g."*
(5) *Case V—Variations of the space, "k" in the CSRR:* Studying the variations of the space *"k,"* showed significant changes in the resonance frequency too. This parameter was found to be very effective in achieving the required resonance frequency of 1.2 GHz. A parametric analysis of *"k"* is shown in Fig. 7(b).

F. Effects of the Substrate and Insulation

Substrate materials with high-permittivity properties are selected for implantable antennas because they shorten the effective wavelength and result in lower resonance frequencies. Correct use of the substrate material is, hence, critical in the design of the implantable antenna. Superstrate layers are, however, used to insulate the implantable antennas from high-permittivity tissue. The operating frequency is reported to be increased by the thicker superstrates, which also increase the physical size to refine the resonance [15]. For implantable antennas, substrates with high permittivity and superstrates with low thicknesses are, hence, the preferred choice. Another method to insulate the antenna is to cover the antenna with a thin layer of low-loss biocompatible coating, as reported in [20] and [72]. In our design, we used Rogers TMM10i substrate with the permittivity $\varepsilon_r = 9.8$, dissipation factor $\tan\delta = 0.0020$, and thickness $t = 1.52$ mm. Also, to keep the overall volume of the antenna to a minimum, a conformal coating was used instead of the superstrate, which did not only insulate the antenna but also helped in reducing the overall size. Effects of the proposed insulation layer, (i.e., the conformal coating) were tested experimentally to observe the changes in the performance of the antenna, but were found nominal.

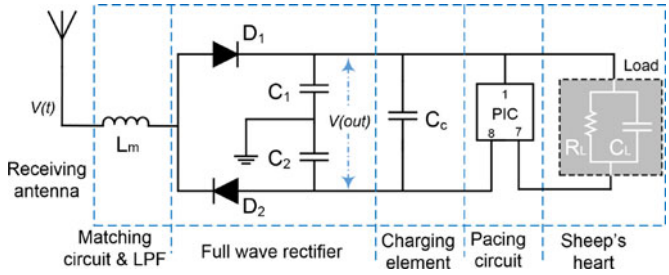

Fig. 8. Complete block diagram with the schematic diagram of the matching circuit, FWR, charging, and pacing circuits.

IV. Rectenna Design

A. Rectifier Topology and Efficiency

As shown in Fig. 8, two half wave rectifiers are combined to make a basic symmetrical voltage multiplier circuit. The addition of a second diode and a capacitor to the output of a standard half-wave rectifier increased its output by a set amount. Since one of the diodes is conducting in each half cycle as in a full-wave rectifier (FWR) circuit, it hence can also be called a full-wave series multiplier [73]. The aforementioned rectifier circuit operates as follows. If *v(t)* is the induced voltage at the antenna port and is positive, then C_1 charges up through diode D_1 and when *v(t)* is negative, capacitor C_2 charges up through diode D_2. The output voltage *v(out)* is taken across the two series-connected capacitors (C_1 and C_2).

The impedance matching stage, as shown in Fig. 8, is essential in providing maximum power transfer from the antenna to the rectifier circuit. Since a rectifier is a nonlinear load with complex impedance that varies with frequency hence, designing the matching network is required. As reported by [74], one design approach is to model the rectifier circuit using experimental characterization at the minimum power level required by the application. This can be achieved by measuring the input impedance of the rectifier circuit without the matching network at that power level. The results of the rectifier's input impedance from the experimental characterization helped in the design of the matching network for 50 Ω. A simple matching circuit comprising of only one inductor (12 nH) was used between the antenna and the rectifier. This inductor also served the purpose of a low-pass filter, allowing RF energy at 1.2 GHz, but rejecting the unwanted higher order harmonics. Also, the use of this filter was necessary to stop the radiation of harmonics generated by the nonlinear diodes, required for the rectification.

Fig. 9 depicts the efficiency η of the full-wave series multiplier circuit, which was measured using the fabricated prototype. The

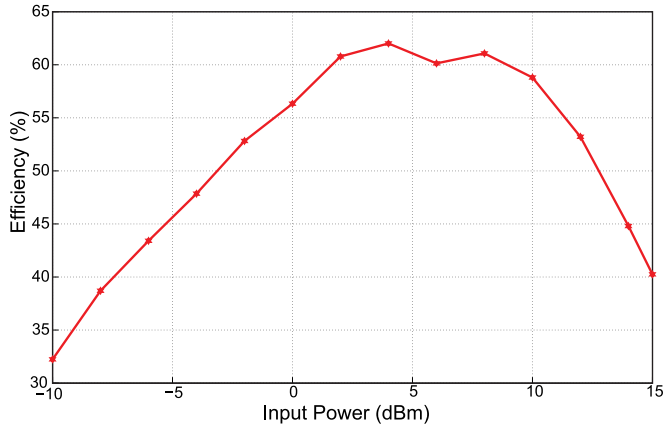

Fig. 9. Measured efficiency (η) of the rectifier circuit at 1.2 GHz.

experimental setup for measuring the η included two horn antennas (HRN-0118, TDK), each used to transmit and receive the continuous sinusoidal signal, generated by the Agilent N5181A (Analog Signal Generator). η was measured as a function of the input RF power from -10 to 15 dBm and calculated using the following formula:

$$\eta = \frac{\text{Harvested Power (DC)}}{\text{Input RF Power to the Rectifier}} = \frac{P_{\text{DC}}}{P_{\text{RF}}} \qquad (2)$$

For most rectifier circuits, η changes with the RF input power, impedance matching, operating frequency, and diode properties. In this study, the operating frequency was kept constant at 1.2 GHz, and also two identical diodes were chosen, while the power was altered to get the efficiency characteristics.

V. Pacing and Charging Circuit

A. Pacing Circuit

The asynchronous, nondemand pacing signal was generated using an 8-bit PIC microcontroller, PIC12LF1840 [75], as shown in Fig. 8. The turn-ON voltage for the microcontroller was 1.8 V, but it was programmed to remain in the sleep mode for the first second. The heart rate of a sedated ovine model has been reported to be 100 bpm [76], so the pacing signal was, hence, generated at a higher rate to observe the changes in the cardiac rhythm. In order to test and overdrive the heart, the selected rates were chosen higher than 100 bpm but not too high to drive the ventricular fibrillation. Measurements of the three sets of successive, but different paced rhythms, generated during this study have been shown in Fig. 10, and summarized as follows:

1) *Rhythm I—110 bpm:* 18 pulses were first generated, as the PIC paced for 1 ms each time, while went to sleep for 544 ms in each cycle. This resulted in (1/ 0.545)$\times$ 60 = 110.1 ($\approx$110) bpm.
2) *Rhythm II—120 bpm:* Next, 20 pulses were generated, where the PIC paced for 1 ms, but remained in sleep mode for 496 ms in each cycle. This combination hence resulted in (1/ 0.496)$\times$ 60 = 120.7 ($\approx$120) bpm.
3) *Rhythm III—130 bpm:* Finally, 22 pulses were generated, where the PIC paced for 1 ms but slept for 456 ms in each cycle. This resulted in (1/ 0.456)$\times$60 = 131.3 ($\approx$130) bpm.

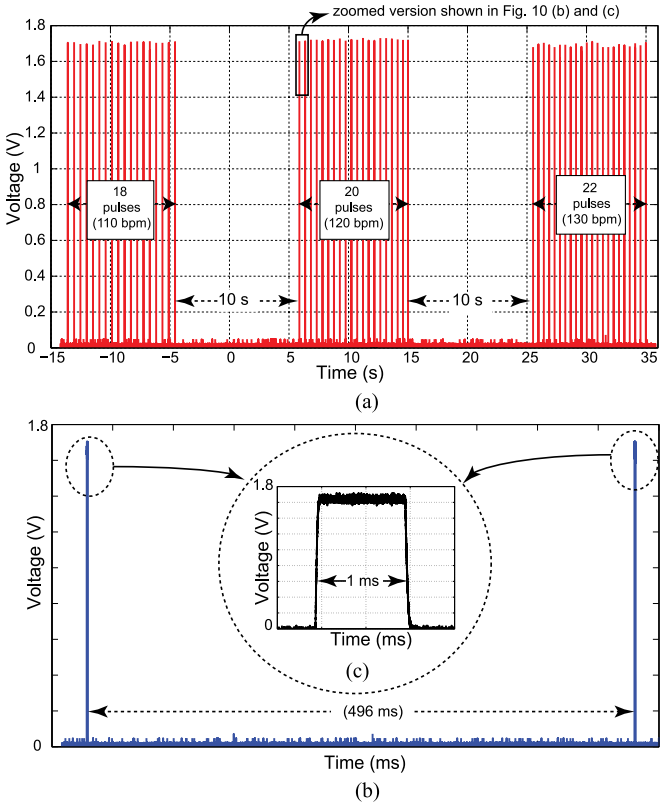

Fig. 10. Measured pacing profile showing, (a) a complete pacing cycle including 18, 20, and 22 pulses, (b) two (out of 20) pulses with the time (496 ms) between them, generating 120 bpm, and (c) profile of a single pulse, its voltage level (1.7 V) and width (1 ms).

B. Charging Circuit and the Load

Next, the output DC voltage of the rectenna was supplied to a bulk capacitor C_c, which was placed across the output of the rectifier circuit and in parallel to the load (which also contains the microprocessor), as shown in Fig. 8. This capacitor charges up when the voltage from the rectifier rises above that of the capacitor and provides the required current from the stored charge, when the rectifier voltage falls. For a FWR, the ripple voltage is estimated using, $V_{\text{ripple}} = I_{\text{load}} / (2fC)$. This equation provides sufficient accuracy for our load, which draws only 30 μA [75]. Although, the capacitor discharge behavior for a purely resistive load is exponential, the inaccuracy introduced by the linear approximation is very small for low values of the ripples. The total load of our system is not only the pacing circuit, but it is the combination of the pacing circuit and the impedance of the heart tissue. A good approximation of the impedance of the heart tissue has hence to be determined.

An initial experiment on the heart of an ovine model was performed to approximate the impedance of the heart tissue. A 100 Ω resistor was connected in series with the heart tissue, using two test probe pins (8 mm apart) inserted at the left ventricle. Next, a digital signal (amplitude = 1 volt, frequency = 5 KHz) was supplied to the series connected resistor and the heart tissue and voltages measured. A complete profile of voltage and current was recorded and finally, a fast Fourier transformation (FFT) was performed on the recorded signals using Ohm's law $(fft(V_{\text{heart}})/fft(I_{100\Omega}))$ to compute the impedance. The fft

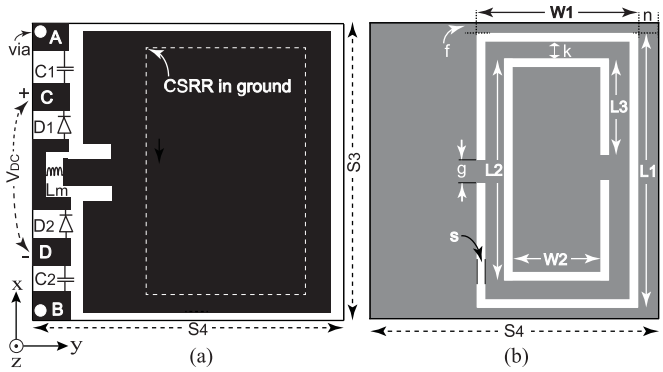

Fig. 11. Complete layout configuration of the rectenna. (a) Top view—antenna matching and the rectifier circuit (D_1,D_2 are the diodes, C_1,C_2 are the capacitors, and L_m is the matching inductor), and (b) bottom view—final geometry of the CSRR. Structure characteristics are (in mm): $g = 0.6$, $f = s = 0.25$, $k = 0.5$, $W_1 = 7.4$, $W_2 = 5$, $L_1 = 9.5$, $L_2 = 8$, $L_3 = 3.7$, $n = 0.4$.

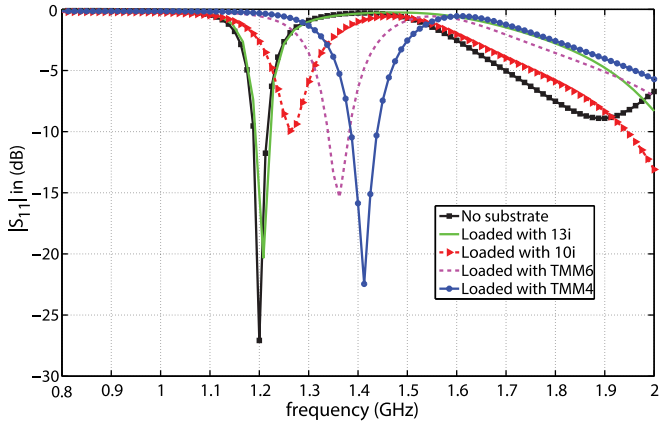

Fig. 12. Study of the dielectric loading of the implantable antenna with different substrates having different permittivity values.

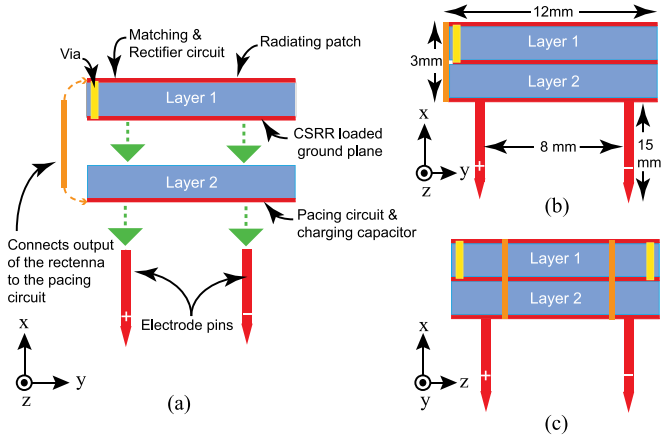

Fig. 13. Assembly process of the prototype. (a) Step-by-step assembly process of the rectenna with the pacing board and the electrode pins. (b) Assembled prototype and its dimensions shown. (c) Different orientation of the assembled prototype, showing the DC voltage connection from the top layer to the bottom of the second layer.

impedance plot showed the spectral contents with 0^{th} harmonic (real impedance) and other higher order harmonics (imaginary impedance). The computed values were found to be, $R = 665\ \Omega$ *and* $C = 59.3$ nF, which was the impedance (approx.) of the heart tissue during the pacing.

VI. Validation and Fabrication of the Battery-Less and Wireless Prototype Implantable Electrode

A. Validation of the Rectenna in HFSS

The implantable antenna designed and discussed in Section III was integrated with the rectifier circuit, discussed in Section IV. To accommodate the rectifier and matching circuit on the same substrate, the overall antenna dimensions were increased by extending the antenna in the -*y* axis (direction) and cutting the microstrip feed short. To validate the design, all the additional components, [i.e., the matching inductor (L_m), the diodes (D_1, D_2), and the capacitors (C_1, C_2)] were simulated as lumped components in HFSS to minimize the error in measurements. This process incurred a mismatch and also shifted the resonance frequency to a higher band. It is to be noted that the size of the radiating patch was not changed and was kept the same as previously mentioned in Fig. 5. The CSRR parameters in the ground plane were finally modified to reachieve a good impedance match at 1.2 GHz. The final layout configuration, together with the rectifier and matching components has been illustrated in Fig. 11.

As depicted in Fig. 11(a), two vias (0.2 mm in radius) were made in pads A and B, to connect the capacitors C_1 and C_2, respectively to the ground. The rectified output DC voltage was received between the pads C and D, which eventually was supplied to the pacing circuit (layer 2) beneath the antenna, as discussed in the Section VI-C.

B. Effects of the Pacing Circuit's Substrate on the Implantable Antenna

As discussed earlier in this section, the pacing circuit had to be glued directly beneath the antenna, making it a two-layer design. The dielectric properties of the pacing circuit board (substrate) would hence strongly influence the performance of the antenna and had hence been analyzed prior to its selection. Various substrates (i.e., TMM4, TMM6, TMM10i, and TMM13i with different dielectric properties, $\varepsilon_r = 4.5, 6.02, 9.8$, and 10.2), respectively were used to study the dielectric loading and results were compared and analyzed. As shown in Fig. 12, the use of TMM13i showed good results and was, hence, finally selected as a substrate for the pacing circuit.

The resonant frequency of the implantable antenna shifted to a higher band, when it was loaded with a substrate of low permittivity values but remained unchanged, when loaded with TMM13i, having $\varepsilon_r = 10.2$. It was observed that the smaller the permittivity of the substrate, the higher the shift in the resonance frequency incurred. As a result, Rogers TMM13i was used for the pacing circuit fabrication.

C. Prototype Fabrication Approach

A step-by-step assembly process of the prototype fabrication approach is shown in Fig. 13(a). As seen in Fig. 13, the rectenna and the matching circuit were fabricated on layer 1, which sat

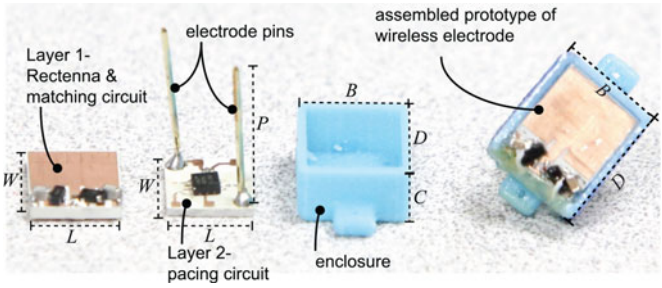

Fig. 14. Various pictures of the fabricated prototype electrode. Dimensions are (in mm): $W = 12$, $L = 10$, $P = 15$, $B = 12.4$, $C = 4.5$, and $D = 14.4$.

TABLE II
DETAILS OF ALL THE COMPONENTS USED

Component / Part	Model / Details
Rectenna substrate	Rogers TMM10i, thickness = 1.52mm, Cu thickness = 35μm, $\varepsilon_r = 9.8$
Pacing circuit substrate	Rogers TMM13i, thickness = 1.52mm, Cu thickness = 35μm, $\varepsilon_r = 10.2$
Capacitors - C_1, C_2	120 pF, SMD 0603-Ceramic, High Q (251R15S221JV4S)
Inductor - L_m	12 nH, 0402, High Frequency- Ceramic, L-07C27NJV6S
Diodes - D_1, D_2	Avago-HSMS 2850 zero bias Schottky detector diode
Capacitor - C_c	4 μF, SMD 0402-Ceramic, High Q (LLL1U4R60G435ME22L), Murata
Microprocessor	PIC12(L)F1840, SMD 8-Pin Flash, Microchip Technology
Pins	Back Probe Pins, Pamona Electronics 6411, 501-1678-ND
Enclosure	Thermoplastic, ABS plus-P430, Stratasys

atop layer 2, containing the pacing circuit and the charging capacitor C_c. As depicted in the Fig. 13(a)–(c), the rectified DC voltage was supplied to the bottom of layer 2, to the charging capacitor, and to supply power to the pacing circuit. Layers 1 and 2 were eventually bonded together using super glue (Loctite). Finally, the back probe pins were soldered in place to the output of the pacing circuit and tips sharpened for easy implantation. The assembled electrode, as shown in Fig. 13(c), was then secured in the 3-D printed enclosure, insulated using a conformal coating, and allowed to dry at room temperature. Various parts of the prototype electrode and a complete manufactured electrode is shown in Fig. 14.

The rectenna as well as the pacing circuit was fabricated using the LPKF milling maching (Protomat S63) on TMM10i and TMM13i, respectively. The 3-D printed enclosure, which houses the antenna and the pacing circuit was designed in Solidworks and printed in house. Details of all the components of the manufactured prototype wireless electrode are shown in Table II.

D. In Vitro Measurements and Results

The final version of the insulated implanted antenna (only, i.e., without the rectifier circuit) was tested in a porcine tissue. All measurements were taken using a calibrated Agilent E5071C ENA Network Analyzer, in an anechoic chamber. The

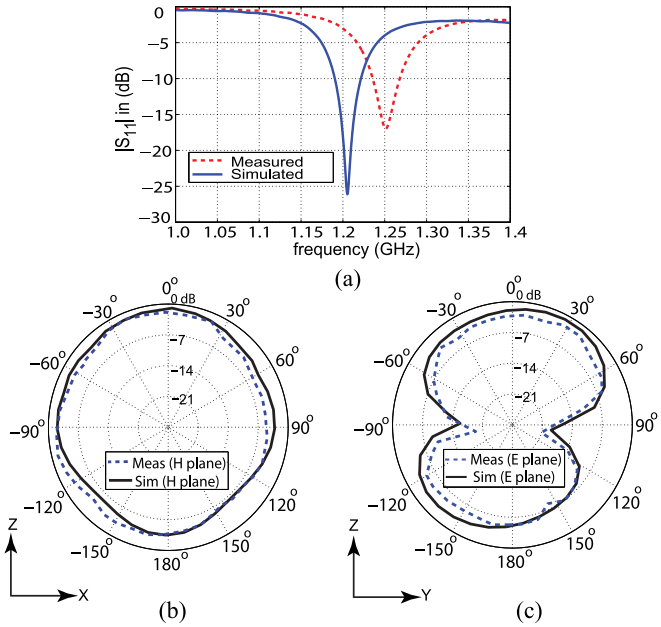

Fig. 15. Simulated and measured (*in vitro*) results of the implantable antenna. (a) Matching performance ($|S_{11}|$), (b) normalized radiation pattern in *xz(H)*-plane, and (c) normalized radiation pattern in *yz(E)*-plane.

measured return loss was compared with the simulations and found in good agreement, as shown in Fig. 15(a). HFSS simulations showed a return loss of −26 dB at 1.2 GHz, while the measured return loss was −17 dB at 1.25 GHz, which showed agreement within 1.04%. Also, simulated and measured normalized radiation patterns in *xz (H)*- and *yz (E)*-planes have been presented in Fig. 15(b) and (c), which showed good agreement. Furthermore, the simulated actual maximum gain and simulated realized gain of the proposed antenna was 0.58 and 0.53 dBi, but the measured realized gain was −1.5 dBi. The slight frequency shift was attributed in part to the fabrication imperfection associated with the resolution of the milling machine and to the difference in electrical properties of the tissue.

VII. MEASUREMENT AND *In Vivo* SURGERIES

To explore how using the ovine subject would affect the performance of the prototype wireless electrode in the human body, collaboration was developed with the Animal Nutrition & Physiology Center (ANPC), North Dakota State University. The *in vivo* measurements were performed in two models, 8 and 4 year old adult of dorset breed. The models weighed 129 and 143 lbs, respectively. Dorset models are often used as research subjects as their cardiac activity and especially the coronory anatomy of their hearts are similar to the anatomy of the human heart. They hence have been a preferred choice for research in the HF treatment [77]. All the surgical procedures and *in vivo* measurements were carried out in accordance with the Institutional Animal Care and Use Committee protocol (No. A15028). For long-term *in vivo* studies, the implantable systems need be enclosed in a medical-grade biocompatible material but a toulene and xylene free conformal coating was used to insulate the implantable electrode in this short-term acute animal study.

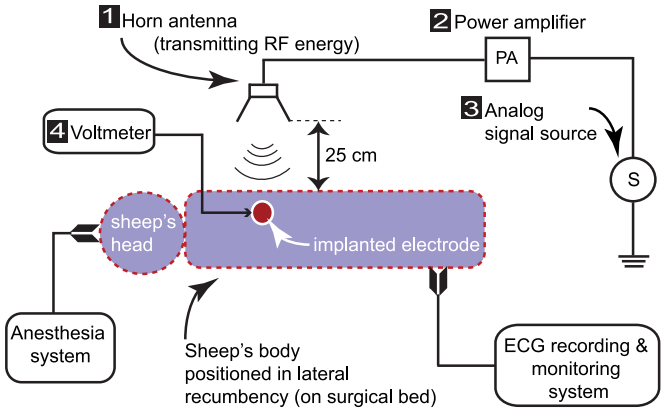

Fig. 16. Layout of the *in vivo* experiment setup and RF energy transmission method with exterior system. Details of the equipment used in the exterior system are: 1 - Horn antenna = TDK-HRN-0118, 2 - Power amplifier = Mini-Circuits (ZHL-30W-252-S+), and 3 - Analog signal source = Agilent-N5181A.

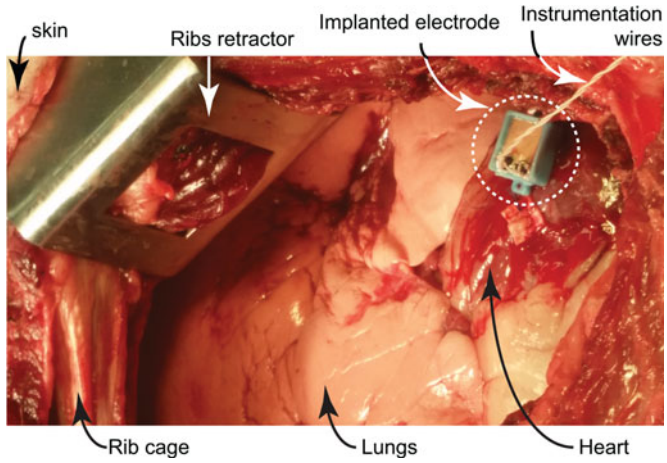

Fig. 17. Picture of the open-thorax of the sheep, showing implanted electrode secured on the epicardial surface with surgical suture. Instrumentation wires, used to monitor the harvested voltage by the implanted electrode can be seen.

A complete blood count and metabolic panel was conducted and examined before the animal was declared fit and suitable to be used for the study. During the surgery, a combination of IV Ketamine (5 mg/kg) and Valium (0.25 mg/kg) were used for the anesthetic induction. In each experiment, the sheep was intubated, with an endotracheal tube and maintained under the anesthesia with Isoflurane (0–5%) under positive ventilation. The sheep was continuously monitored to assure surgical plane of anesthesia by heart rate, blood pressure, respiratory rate, O_2 saturation, and capnometry (exhaled CO_2 levels) at 35–45 mmHg as well as jaw tone, ocular, and palpebral reflexes.

Following adequate general anesthesia, the ovine subject was positioned in the right lateral decubitus (recumbency) position and an antero-lateral left thoracotomy was performed. To gain access to the left thorax, the extremities were positioned and held in place using rope. The left chest was shaved with a no. 40 clipper blade and three alternating scrubs using betadine followed by an alcohol rinse were used to prep the surgical site. After site preparation, surgical drapes and lighting were setup and incandescent lights were used to maintain the body temperature.

For *in vivo* studies, our experimental and surgical setup, shown in Fig. 16, consists of the ovine test subject, horn antenna, power amplifier, signal generator, and a voltmeter. The implantation of our wireless electrode began with the incision made on the front and left side of the chest of the selected model. The incision was carried down to the ribs using a muscle splitting technique and the seventh interspace was entered into the pleural space. Next, the pericardium was incised vertically and the heart was delivered into the pleural space, taking care not to compromise venous return. Cautery was disconnected at this time to avoid damage to the electrode once it was implanted.

The heart was examined and a clear area was located to the left of the LAD (left anterior descending coronary artery), on the epicardial surface of the left ventricle. This flat area above the apex was selected to insert the electrode pins directly into the myocardium. Two previously placed nonconductive pledgeted prolene 5–0 sutures were placed through small plastic loops, located on the sides of the electrode's enclosure for stabilization. Instrumentation wires from the electrode were gently brought through the medial aspect of the thoracotomy to monitor the rectified voltage harvested by the implanted electrode, as shown in Fig. 17. Once the electrode was implanted and secured, a rib approximator was used to complete the cardiothoracic procedure and the chest was sealed with a vicryl (Ethicon, Inc.) suture.

VIII. Results and Discussion

The results from the *in vivo* studies validated the ability of the wireless electrode, implanted deep inside the body of the model to receive the RF energy and harvest it to provide enough power for the microprocessor to provide pacing. As shown in the layout (see Fig. 16), the horn antenna was placed approximately 25 cm above the thorax and supplied the RF energy to the implanted pacemaker. The distance of 25 cm was the maximum allowed to power and interrogate the implant under the safe level of RF exposure, as summarized in [78]. In our *in vivo* studies, pacing at three different rates, 110, 120, and 130 bpm were achieved and demonstrated. These results were measured live and saved using a six lead ECG module connected to the ovine model during the course of the experiment. Some results are shown in Fig. 18. IEEE limits for the maximum permissible exposure (MPE) in the controlled environment [78] were followed and the safe power density at the operating frequency of 1.2 GHz was computed as, $1200\,\text{MHz}/1500 = 0.8\,\text{mW/cm}^2$.

In our experimental setup, the power density S, incident on the surface of the thorax was computed using the following formula [79]:

$$S = \frac{G_t P_t}{4\pi R^2} \tag{3}$$

$G_t (= 6.5\ \text{dBi})$ was the gain of the horn antenna at 1.2 GHz, while P_t $(= 10\ \text{dBm})$ was the approximate power transmitted from the horn, which also included the gain of the power amplifier. R was the distance between the horn and the thorax, which was measured to be 25 cm (approx). The power density using these values was computed to be $0.0082\ \text{mW/cm}^2$, which was well under the required safe level, and, hence met the MPE specifications.

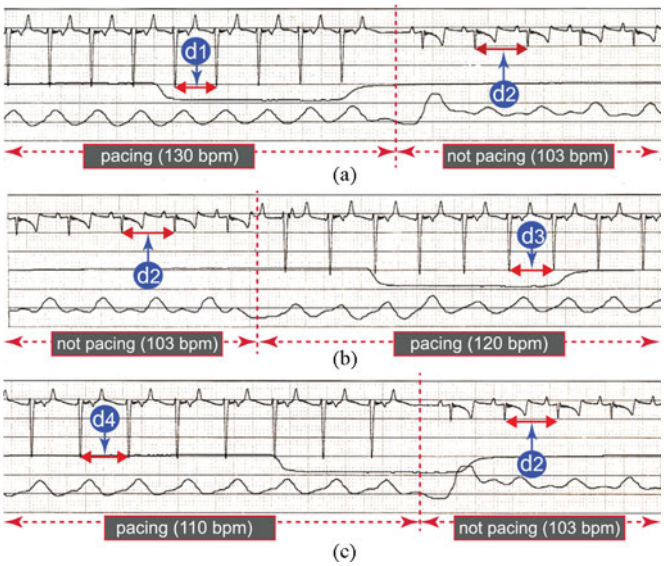

Fig. 18. ECG results showing native heartbeat, as well as pacing achieved at different rates, i.e., (a) 130 bpm ($d_1 = 11.5$ mm (≈ 0.46 s), and $d_2 = 14.5$ mm (≈ 0.58 s)), (b) 120 bpm ($d_3 = 12.5$ mm (≈ 0.49 s)), and (c) 110 bpm ($d_4 = 13.5$ mm (≈ 0.54 s)). Paper speed is 25 mm/s.

Energy transmission using a horn antenna, held on the top of a subject might not seem practical, but the aim of this study was to prove the concept of the wireless energy transfer *in vivo* and the feasibility of wireless cardiac pacing. It is envisioned that the clinical use of our system will require: (a) a wearable battery operated transmitter system with a miniaturized conformal antenna, and (b) a miniaturized cylindrical-shaped biocompatible electrode that can be fully inserted into the myocardium. Furthermore, the operation frequency of 1.2 GHz was used because a set of preliminary experiments indicated that this frequency produced good propagation through the tissue and also, this frequency matched efficient performance of the available Schottky diodes, which resulted in a more efficient rectifier circuit.

IX. Conclusion and Future Work

This paper considers the problem of leads and batteries required for the conventional cardiac pacemakers and presents the design and *in vivo* test of a batteryless and fully wireless implantable asynchronous cardiac pacemaker. The prototype implanted electrode has been successfully tested on the left ventricle of an ovine model. It is shown that a small implanted pacemaker can be wirelessly powered using an external RF source and can provide leadless pacing. Pacing at three different rates (110, 120, 130 bpm) has been achieved and demonstrated in this study. This proposed RF powered wireless cardiac system employs a unique technique, which completely eliminates the use of the leads and batteries in cardiac pacing. This method provides a new frontier of research in wireless cardiac pacing, which may be extended to other areas in the wireless biomedical sensors. Once clinically proven, this technology has the potential to allow multiple electrodes to be implanted in the heart, without the need for any leads or batteries.

Future study will include further miniaturization, and also the design and test of the electrode for Industrial, Scientific, and Medical bands. Moreover, we will investigate the efficiency of the CSRR antenna for different subjects and study its effects on the pacemaker performance.

Acknowledgment

The authors would like to thank J. Hayden (Research Compliance Administrator) and the surgical support team at the ANPC, NDSU for their excellent support during this project.

References

[1] Centers for Disease Control and Prevention. Atlanta, GA, USA. (2015, Apr.). [Online]. Available: http://www.cdc.gov/heartdisease/facts.htm
[2] K. L. Lee, "In the wireless era: Leadless pacing," *Expert Rev. Cardiovascular Therapy*, vol. 8, no. 2, pp. 171–174, 2010.
[3] R. E. Kirkfeldt *et al.*, "Risk factors for lead complications in cardiac pacing: A population-based cohort study of 28,860 Danish patients," *Heart Rhythm*, vol. 8, no. 10, pp. 1622–1628, 2011.
[4] R. G. Hauser *et al.*, "Clinical experience with pacemaker pulse generators and transvenous leads: An 8-year prospective multicenter study," *Heart Rhythm*, vol. 4, no. 2, pp. 154–160, 2007.
[5] M. Haghjoo *et al.*, "Predictors of venous obstruction following pacemaker or implantable cardioverter-defibrillator implantation: A contrast venographic study on 100 patients admitted for generator change, lead revision, or device upgrade," *Europace*, vol. 9, pp. 328–332, 2007.
[6] R. G. Hauser *et al.*, "Risk factors for infection of implantable cardiac devices: Data from a registry of 2496 patients," *Europace*, vol. 15, no. 1, pp. 66–70, 2012.
[7] S. Pakarinen *et al.*, "Short-term implantation-related complications of cardiac rhythm management device therapy: A retrospective single-centre 1-year survey," *Europace*, vol. 12, no. 1, pp. 103–108, 2009.
[8] N. Derval *et al.*, "Optimizing hemodynamics in heart failure patients by systematic screening of left ventricular pacing sites: The lateral left ventricular wall and the coronary sinus are rarely the best sites," *J. Amer. College Cardiol.*, vol. 55, no. 6, pp. 566–575, 2010.
[9] Live science-Human heart diagram. (2015, Apr.). [Online]. Available: http://www.livescience.com/44105-respiratory-system-surprising-facts.ht ml
[10] L. Cammilli *et al.*, "Radio-frequency pacemaker with receiver coil implanted on the heart," *Ann. New York Acad. Sci.*, vol. 111, pp. 1749–6632, 1964.
[11] W. D. Widmann *et al.*, "Radio-frequency cardiac pacemaker," *Ann. New York Acad. Sci.*, vol. 111, pp. 992–1006, 1964.
[12] A. Auricchio *et al.*, "First-in-man implantation of leadless ultrasound-based cardiac stimulation pacing system: Novel endocardial left ventricular resynchronization therapy in heart failure patients," *Europace*, vol. 15, no. 8, pp. 1191–1197, 2013.
[13] St. Jude Medical, Inc. Saint Paul, MN, USA. (2015, Mar.). [Online]. Available: http://sjm.com/leadlesspacing
[14] Medtronic, Inc. Fridley, MN, USA. (2015, Mar.). [Online]. Available: http://www.medtronic.com
[15] A. Kiourti and K. Nikita, "A review of implantable patch antennas for biomedical telemetry: Challenges and solutions [wireless corner]," *IEEE Antennas Propag. Mag.*, vol. 54, no. 3, pp. 210–228, Jun. 2012.
[16] E. Chow *et al.*, "Implantable RF medical devices: The benefits of high-speed communication and much greater communication distances in biomedical applications," *IEEE Microw. Mag.*, vol. 14, no. 4, pp. 64–73, Jun. 2013.
[17] M. Hannan *et al.*, "Energy harvesting for the implantable biomedical devices: Issues and challenges," *BioMed. Eng. Online*, vol. 13, no. 79, pp. 1–23, Jun. 2014.
[18] J. Kim and Y. Rahmat-Samii, "Implanted antennas inside a human body: Simulations, designs, and characterizations," *IEEE Trans. Microw. Theory Techn.*, vol. 52, no. 8, pp. 1934–1943, Aug. 2004.
[19] P. Soontornpipit *et al.*, "Design of implantable microstrip antenna for communication with medical implants," *IEEE Trans. Microw. Theory Techn.*, vol. 52, no. 8, pp. 1944–1951, Aug. 2004.
[20] A. Kiourti and K. S. Nikita, "Implantable antennas: A tutorial on design, fabrication, and in vitro/in vivo testing," *IEEE Microw. Mag.*, vol. 15, no. 4, pp. 77–91, Jun. 2014.
[21] C. Furse, "Designing of an antenna for pacemaker communication," *Microw. RF*, vol. 39, no. 3, pp. 73–76, Mar. 2000.
[22] J. Schuster and R. Luebbers, "An FDTD algorithm for transient propagation in biological tissue with a Cole–Cole dispersion relation," in *Proc.*

IEEE Int. Symp. Antennas Propag., Atlanta, GA, USA, Jun. 1998, vol. 4 pp. 1988–1991.
[23] S. Soora *et al.*, "A comparison of two and three dimensional dipole antennas for an implantable retinal prosthesis," *IEEE Trans. Antennas Propag.*, vol. 56, no. 3, pp. 622–629, Mar. 2008.
[24] K. Takahata *et al.*, "Micromachined antenna stents and cuffs for monitoring intraluminal pressure and flow," *J. Microelectromech. Syst.*, vol. 15, no. 5, pp. 1289–1298, Oct. 2006.
[25] E. Chow *et al.*, "Evaluation of cardiovascular stents as antennas for implantable wireless applications," *IEEE Trans. Microw. Theory Techn.*, vol. 57, no. 10, pp. 2523–2532, Oct. 2009.
[26] N. Cho *et al.*, "A planar MICS band antenna combined with a body channel communication electrode for body sensor network," *IEEE Trans. Microw. Theory Techn.*, vol. 57, no. 10, pp. 2515–2522, Oct. 2009.
[27] C. Liu *et al.*, "Compact dual-band antenna for implantable devices," *IEEE Antennas Wireless Propag. Lett.*, vol. 11, pp. 1508–1511, Dec. 2012.
[28] C.-M. Lee *et al.*, "Dual-resonant pi-shape with double l-strips pifa for implantable biotelemetry," *Electron Lett.*, vol. 44, pp. 1508–1511, Jul. 2008.
[29] T. Yilmaz *et al.*, "Characterization and testing of a skin mimicking material for implantable antennas operating at ism band (2.4 GHz–2.48 GHz)," *IEEE Antennas Wireless Propag. Lett.*, vol. 7, pp. 418–420, Jun. 2008.
[30] W. Xia *et al.*, "Performances of an implanted cavity slot antenna embedded in the human arm," *IEEE Trans. Antennas Propag.*, vol. 57, no. 4, pp. 894–899, Apr. 2009.
[31] P. Izdebski *et al.*, "Conformal ingestible capsule antenna: A novel chandelier meandered design," *IEEE Trans. Antennas Propag.*, vol. 57, no. 4, pp. 900–909, Apr. 2009.
[32] E. Falkenstein *et al.*, "Low-power wireless power delivery," *IEEE Trans. Microw. Theory Techn.*, vol. 60, no. 7, pp. 2277–2286, Jul. 2012.
[33] M. Theodoridis and S. Mollov, "Distant energy transfer for artificial human implants," *IEEE Trans. Biomed. Eng*, vol. 52, no. 11, pp. 1931–1938, Nov. 2005.
[34] M. Catrysse *et al.*, "An inductive power system with integrated bidirectional data-transmission," *Sens. Actuators A, Phys.*, vol. 115, nos. 2/3, pp. 221–229, 2004.
[35] U.-M. Jow and M. Ghovanloo, "Design and optimization of printed spiral coils for efficient transcutaneous inductive power transmission," *IEEE Trans. Biomed. Circuits Syst.*, vol. 1, no. 3, pp. 193–202, Sep. 2007.
[36] L.-J. Xu *et al.*, "Miniaturized circularly polarized loop antenna for biomedical applications," *IEEE Trans. Antennas Propag.*, vol. 63, no. 3, pp. 922–930, Mar. 2015.
[37] Z. Harouni *et al.*, "A dual circularly polarized 2.45-GHz rectenna for wireless power transmission," *IEEE Antennas Wireless Propag. Lett.*, vol. 10, pp. 306–309, Apr. 2011.
[38] M. Ali *et al.*, "A new circularly polarized rectenna for wireless power transmission and data communication," *IEEE Antennas Wireless Propag. Lett.*, vol. 4, pp. 205–208, Aug. 2005.
[39] H. Sun *et al.*, "Design of a high-efficiency 2.45-GHz rectenna for low-input-power energy harvesting," *IEEE Antennas Wireless Propag. Lett.*, vol. 11, pp. 929–932, Aug. 2012.
[40] J. Akkermans *et al.*, "Analytical models for low-power rectenna design," *IEEE Antennas Wireless Propag. Lett.*, vol. 4, pp. 187–190, Jun. 2005.
[41] A. G. Vera *et al.*, "Design of a 2.45 GHz rectenna for electromagnetic (EM) energy scavenging," in *Proc. IEEE Symp. Radio Wireless*, New Orleans, LA, USA, Jan. 2010, pp. 61–64.
[42] L. Marnat *et al.*, "On-chip implantable antennas for wireless power and data transfer in a Glaucoma-Monitoring SoC," *IEEE Antennas Wireless Propag. Lett.*, vol. 11, pp. 1671–1674, Jan. 2012.
[43] F.-J. Huang *et al.*, "Rectenna application of miniaturized implantable antenna design for triple-band biotelemetry communication," *IEEE Trans. Antennas Propag.*, vol. 59, no. 7, pp. 2646–2653, Jul. 2011.
[44] S. Hu *et al.*, "A low-cost 2.45-GHz wireless power link for biomedical devices," in *Proc. IEEE Asia-Pacific Conf. Antennas Propag.*, Singapore, Aug. 2012 pp. 215–216.
[45] A. Poon *et al.*, "Optimal frequency for wireless power transmission into dispersive tissue," *IEEE Trans. Antennas Propag.*, vol. 58, no. 5, pp. 1739–1750, May. 2010.
[46] C. Liu *et al.*, "Design and safety considerations of an implantable rectenna for far-field wireless power transfer," *IEEE Trans. Antennas Propag.*, vol. 62, no. 11, pp. 5798–5806, Nov. 2014.
[47] S. Yang and J. Kim, "Wireless power transmission using dipole rectennas made on flexible cellulose membrane," *IET Microw. Antenna Propag.*, vol. 6, no. 7, pp. 756–760, May 2012.
[48] M. K. Hosain *et al.*, "A miniature energy harvesting rectenna for operating a head-mountable deep brain stimulation device," *IEEE Access*, vol. 3, pp. 223–234, Jan. 2015.
[49] E. Chow *et al.*, "Fully wireless implantable cardiovascular pressure monitor integrated with a medical stent," *IEEE Trans. Biomed. Eng.*, vol. 57, no. 6, pp. 1487–1496, Jun. 2010.
[50] InnerBody. (2015, Apr.). [Online]. Available: http://www.innerbody.com
[51] T. Dissanayake *et al.*, "Dielectric loaded impedance matching for wide-band implanted antennas," *IEEE Trans. Microw. Theory Techn.*, vol. 57, no. 10, pp. 2480–2487, Oct. 2009.
[52] F. Merli *et al.*, "The effect of insulating layers on the performance of implanted antennas," *IEEE Trans. Antennas Propag.*, vol. 59, no. 1, pp. 21–31, Jan. 2011.
[53] P. S. Hall and Y. Hao, *Antennas and Propagation for Body-Centric Wireless Communications*. Norwood, MA, USA: Artech House, 2012, pp. 63–107.
[54] S. Best and J. Morrow, "On the significance of current vector alignment in establishing the resonant frequency of small space-filling wire antennas," *IEEE Antennas Wireless Propag. Lett.*, vol. 2, no. 1, pp. 201–204, Feb. 2003.
[55] W. Scanlon *et al.*, "Radiowave propagation from a tissue-implanted source at 418 MHz and 916.5 MHz," *IEEE Trans. Biomed. Eng.*, vol. 47, no. 4, pp. 527–534, Apr. 2000.
[56] K. Ito, "Human body phantoms for evaluation of wearable and implantable antennas," in *Proc. 2nd Eur. Conf. Antennas Propag.*, Edinburgh, U.K., Nov. 2007, pp. 1–6.
[57] K. Ito *et al.*, "Development and characteristics of a biological tissue-equivalent phantom for microwaves," *Electron. Commun. Jpn.*, vol. 84, no. 4, pp. 1–6, 2001.
[58] T. Karacolak *et al.*, "Design of a dual-band implantable antenna and development of skin mimicking gels for continuous glucose monitoring," *IEEE Trans. Microw. Theory Techn.*, vol. 56, no. 4, pp. 1001–1008, Apr. 2008.
[59] Y. Okano *et al.*, "The SAR evaluation method by a combination of thermographic experiments and biological tissue-equivalent phantoms," *IEEE Trans. Microw. Theory Techn*, vol. 48, no. 11, pp. 2094–2103, Nov. 2000.
[60] *ETSI Standard, Electromagnetic Compatibility and Radio Spectrum Matters (ERM); Ultra Low Power Active Medical Implants (ULP-AMI) Operating in the 401 MHz to 402 MHz and 405 MHz to 406 MHz Bands; System Reference Document*, vol. V1.1.1, no. TR 102 343, 2004.
[61] C. Gabriel, "Compilation of the dielectric properties of body tissues at RF and microwave frequencies," Brooks Air Force, San Antonio, TX, USA, Tech. Rep. N.AL/OE-TR-31-CB, 1996.
[62] C. Gabriel *et al.*, "The dielectric properties of biological tissues," *Phys. Med. Biol.*, vol. 41, no. 11, pp. 2231–2293, 1996.
[63] F. Merli *et al.*, "Design, realization and measurements of a miniature antenna for implantable wireless communication systems," *IEEE Trans. Antennas Propag.*, vol. 59, no. 10, pp. 3544–3555, Oct. 2011.
[64] J. Baena *et al.*, "Equivalent-circuit models for split-ring resonators and complementary split-ring resonators coupled to planar transmission lines," *IEEE Trans. Microw. Theory Techn.*, vol. 53, no. 4, pp. 1451–1461, Apr. 2005.
[65] S. Raghavan and V. Rajeshkumar, "An overview of metamaterials in biomedical applications," in *Proc. Conf. Progress Electromagn. Res. Symp.*, Mar. 2013, pp. 368–371.
[66] M.-C. Tang and R. Ziolkowski, "A study of low-profile, broadside radiation, efficient, electrically small antennas based on complementary split ring resonators," *IEEE Trans. Antennas Propag.*, vol. 61, no. 9, pp. 4419–4430, Sep. 2013.
[67] L. Desclos *et al.*, "Patch antenna size reduction by combining inductive loading and short-points technique," *Microw. Opt. Technol. Lett.*, vol. 30, no. 6, pp. 385–386, Feb. 2001.
[68] K. Rajab *et al.*, "Size reduction of microstrip patch antennas with left-handed transmission line loading," *IET Microw. Antenna Propag.*, vol. 1, no. 1, pp. 39–44, Feb. 2007.
[69] Y. Dong *et al.*, "Design and characterization of miniaturized patch antennas loaded with complementary split-ring resonators," *IEEE Trans. Antennas Propag.*, vol. 60, no. 2, pp. 772–785, Feb. 2012.
[70] S. Gupta and G. Mumcu, "Circularly polarised printed antenna miniaturised using complementary split-ring resonators and reactive pin loading," *IET Microw. Antenna Propag.*, vol. 9, no. 2, pp. 118–124, 2015.
[71] X. Cheng *et al.*, "A compact omnidirectional self-packaged patch antenna with complementary split-ring resonator loading for wireless endoscope applications," *IEEE Antennas Wireless Propag. Lett.*, vol. 10, pp. 1532–1535, Dec. 2011.

[72] L. Kneisz *et al.*, "The short-term effects of antenna insulation thickness on path losses in wireless telemetry implants at microwave frequencies," *Eur. J. Transl. Myol.*, vol. 23, pp. 91–94, 2013.
[73] S. H. Ward, Ed. 87th, *The ARRL Handbook for Radio Communications*. Newington, CT, USA: ARRL, 2010.
[74] U. Olgun et al.,"Low-profile planar rectenna for batteryless RFID sensors," in *Proc. IEEE Int. Symp. Antennas Propag.*, Toronto, ON, Canada, Jul. 2010, pp. 1–4.
[75] Microschip Technology, Inc. (2015, Apr.). [Online]. Available: http://www.microschip.com
[76] K.W. Clarke *et al.*, "Section 2: Anaesthesia of the species," in *Veterinary Anaesthesia*. Amsterdam, The Netherlands: Elsevier, 2014, pp. 345–384.
[77] E. Monnet and J. Chachques, "Animal models of heart failure: What is new?" *Ann. Thoracic Surg.*, vol. 79, pp. 1445–1453, 2004.
[78] *IEEE Standard for Safety Levels with Respect to Human Exposure to Radio Frequency Electromagnetic Fields, 3 kHz to 300 GHz*, IEEE Standard C95.1-2005, 2006.
[79] W. L. Stutzman and G. A. Thiele, *Antenna Theory and Design*. 3rd ed. New York, NY, USA: Wiley, 2012, pp. 100–127.

Sajid M. Asif (S'07) received the B.S. degree in electrical engineering (communication) from the University of Engineering and Technology, Taxila, Pakistan, in 2004, and the M.S. degree in radio frequency communication engineering from the University of Bradford, Bradford, U.K., in 2006. He is currently working toward the Ph.D. degree at the Department of Electrical and Computer Engineering, North Dakota State University, Fargo, ND, USA.

From 2011 to 2013, he was a Faculty Member in the Department of Electrical Engineering, COMSATS Institute of Information Technology, Attock, Pakistan. He is currently serving as the Chair of the IEEE Red River Valley (RRV) section and previously served as the Vice Chair of the RRV section from April 2014 to June 2015. His research interests include RF/Microwave circuits, printed antennas, antennas for RFID tags, wireless sensors, and energy harvesting for biomedical applications.

Mr. Asif received the the US National Science Foundation funded ND-EPSCOR Doctoral Dissertation Assistantship Award for 2015.

Jared Hansen (S'15) was born in Minneapolis, MN, USA, in 1989. He received the Bachelor's degree in electrical engineering from North Dakota State University, Fargo, ND, USA, in 2013, where he is currently working toward the Master's degree in electrical engineering.

His research interests include electromagnetic field exposure and gene expression, computational animal modeling, and wireless pacemaker technology.

Muhammad S. Khan (S'14) received the B.S. degree in electrical (telecom) engineering from COMSATS Institute of Information Technology, Islamabad, Pakistan, in 2011. He is currently working toward the Ph.D. degree in information engineering at the University of Padova, Padova, Italy.

He received the EMMA WEST Exchange Scholarship for the B.Sc. mobility program. He also received the fully funded Ph.D. scholarship. From 2014 to 2015, he was a Visiting Researcher at North Dakota State University, Fargo, ND, USA. His current research interests include MIMO antennas, and design and applications of ultra-wideband antennas.

Scott D. Walden received the Doctor of Veterinary Medicine (DVM) degree from the College of Veterinary Medicine, Iowa State University, Ames, IA, USA, in 1995.

He held a Postdoctoral Research position at Coulston Foundation, Alamogordo, NM, USA, from 1996 to 1997. He has vast experience and worked in several positions including Clinical, Consulting, Area, and IACUC Attending Veterinarian. He also worked as an Animal Caretaker and as an Instructor. He has currently an active Veterinary license for the State of North Dakota and previously had similar licenses from the States of Minnesota and Iowa. He is the Director of Animal Resources at North Dakota State University, Fargo, ND, USA, and is also the University Attending Veterinarian since 2007.

Dr. Walden received various awards including the H.M. Halverson Scholarship, the National Dean's List, and the Robert W. Carithers Award.

Mark O. Jensen received the B.A. Magna Cum Laude degree in chemistry and biology from Augustana College, Sioux Falls, SD, USA, and the M.D. degree from the University of Minnesota School of Medicine, Minneapolis, MN, USA, and completed his general surgery residency at Hennepin County Medical Center, Minneapolis, MN, USA.

He joined the faculty of the University of North Dakota, Fargo, ND, USA, in 1987 as a Clinical Assistant Professor of Surgery and became a Full Professor of Surgery on July 1, 2000. He was the Chief of Surgical Services at the VA Medical Center in Fargo, ND, USA, for 20 years, and former Flight Surgeon in the Army/Air Force. He is Board Certified in General Surgery with special interests in surgical oncology. He is a Professor of Surgery in the Department of Surgery, University of North Dakota School of Medicine and Health Sciences, Grand Forks, ND, USA. He is the Director of UND Division of Surgical Anatomy. He is also an Extra Class ham radio operator and builds his radios.

Benjamin D. Braaten (S'02–M'09–SM'14) received the Ph.D. degree in electrical engineering from North Dakota State University, Fargo, ND, USA, in 2009.

During the 2009 Fall semester, he held a Postdoctoral Research position at the South Dakota School of Mines and Technology in Rapid City, SD, USA. He is currently an Associate Professor in the Department of Electrical and Computer Engineering, North Dakota State University. His research expertise include printed antennas, conformal selfadapting antennas, microwave devices, topics in EMC, and methods in computational electromagnetics.

Dr. Braaten received the College of Engineering and Architecture Graduate Researcher of the Year Award. He also serves as an Associate Editor for the IEEE ANTENNAS AND WIRELESS PROPAGATION LETTERS.

Daniel L. Ewert received the Ph.D. degree in physiology from the University of North Dakota, Fargo, ND, USA, in 1989.

Since 1990, he has been a Professor of electrical and computer engineering at North Dakota State University, Fargo, ND, USA. He was also the Chair of the same department from 2001 to 2009. From 2010 to 2011, he was the Director of Iron Range Engineering program at Minnesota State University, Mankato, MN, USA. From 1989 to 1990, he held a Postdoctoral Research position at Mayo Clinic. He has performed cardiovascular engineering research with the US Air Force, NASA, Russian Space Agency, Birmingham Children's Hospital, England, and University of Louisville. He is the Founder and CEO of Krisara Engineering; a medical device start-up company. His research interests include cardiovascular engineering and wireless biomedical sensors.